Springer

Journal of
Mechanical
Science and
Technology

Journal of Mechanical Science and Technology 22 (2008) 2~11

www.springerlink.com/content/1738-494x

New sidewall contour for evaluation of sidewall's rotational stiffness of a radial tire

Yong-woo Kim*

Department of Mechanical Engineering, Sunchon National University, Chonnam 540-742, Korea

(Manuscript Received August 18, 2006; Revised July 31, 2007; Accepted August 1, 2007)

Abstract

In this paper, we revisit the netting theory for the estimation of the rotational stiffness of sidewall of radial tires and suggest a new sidewall contour for evaluation of the rotational stiffness due to cord tension since the conventional theoretical curve does not fit the real curve in the interval near to a bead point. A new sidewall contour is constructed by combining the conventional curve in the interval near to the tread end and the quadratic curve in the interval near to the bead point. The new sidewall contour makes it possible to represent the real sidewall contour more accurately than the conventional one. The netting analysis using the new sidewall contour yields improved stiffness. We have illustrated the above facts by applying the new sidewall contour to a radial tire of P205/60R15 and have compared its rotational stiffness with an experimental one.

Keywords: Radial tire; Rotational stiffness of sidewall; Carcass cord; Netting theory; Theoretical sidewall contour; Cord tension

1. Introduction

Modern tire structures have evolved through a series of modifications of the original pneumatic rubber tire. These modifications were based on field experiences and on mostly experimental studies of tire behavior. The use of mathematical analysis to calculate tire stresses and deformations remained limited in scope for a long time because of the complexity of tire structure [1, 2].

It is worthwhile to use a simpler tire model of "spring bedded ring model", which consists of the sidewall and tread including the belt structure. This simple model has been used effectively since Fiala [3] gave an explicit formula for cornering characteristics of a running tire. It has been applied to investigations on riding comfort [4], vibration [5-10], standing wave phenomena [11, 12], contact pressure distribution [13], and rolling resistance14]. Akasaka et al. [15] have given an analytical method for estimating the sidewall's rotational stiffness of radial tires. They have proposed a sidewall contour to calculate the stiffness of the sidewall. Kim et al. [16, 17] have suggested an analytical method based on Akasaka's netting theory with his sidewall contour equation to estimate the lateral [16] and the rotational [17] stiffness of the rubber sheet of a sidewall by using the equivalent elastic constant of the constituent rubber compounds.

In this paper, we have considered Akasaka's calculation of the rotational stiffness of the sidewall [15]. According to them, the rotational stiffness of a spring bedded ring model consists of two parts. One is the stiffness due to cord tension which is caused by inflation pressure, the other is the stiffness due to the rubber sheet. In spite of their excellent contribution, there still remains the weakness that their theoretical curve does not fit the real curve in the interval between the modified bead point and a certain point that is located between the modified bead point and the turning point. The curve is closely related to the rotational stiffness

*Corresponding author. Tel.: +82 61 750 3536, Fax.: +82 61 750 3530
E-mail address: kyw@sunchon.ac.kr
DOI 10.1007/s12206-007-1001-1

due to cord tension. Focusing on the curve itself and the rotational stiffness based on the curve, this paper presents a new sidewall contour that is closer to the real one than the conventional one. Applying the netting theory based on the new sidewall contour to a radial tire of P205/60R15, we have compared its rotational stiffness with conventional one and experimental one.

2. Rotational stiffness of sidewall

The rotational stiffness of the sidewall is defined as

$$R = \frac{T}{\psi} \tag{1}$$

when the tread is fixed as shown in Fig. 1.

Assuming that the sidewall is a composite toroidal membrane structure under inflation pressure p and considering that the sidewall is composed of fiber-reinforced laminates with rubber compound matrix as shown in Fig. 2, we can assume that they share in the applied torque T in the manner of

$$T = T(c) + T(s) \tag{2}$$

where $T(c)$ is the torque shared by the carcass cord and $T(s)$ is the torque shared by the rubber sheet.

If the cord is inextensible, it will deform the contour of sidewall in a manner that the section width is decreased slightly as shown in Fig. 3. Therefore, $T(c)$ is expressed as

$$T(c) = 2(n)(t)(r_D \cos\alpha_D) \tag{3}$$

where n is the cord end count and t is cord tension under inflation pressure p. The factor of 2 is multiplied since there are two sidewalls.

Let N denote the shear force per thickness of sidewall on the cross-section at r, then $T(s)$ is expressed by

$$T(s) = 2(2\pi rN)(r) \tag{4}$$

From Eqs. (1) and (2),

$$R = \frac{T(c) + T(s)}{\psi} = R(c) + R(s) \tag{5}$$

where $R(c) = T(c)/\psi$ and $R(s) = T(s)/\psi$.

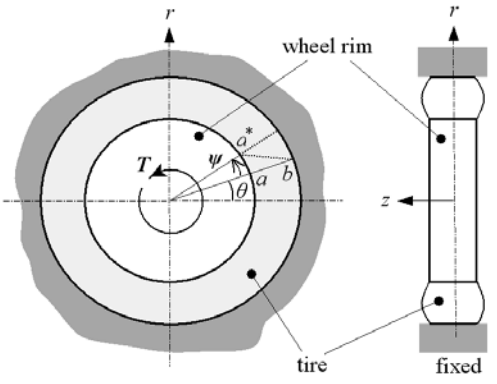

Fig. 1. Applied torque (T) and the rotational angle (ψ); the line $\overline{ab}$ before deformation becomes $\overline{a^*b}$ after deformation.

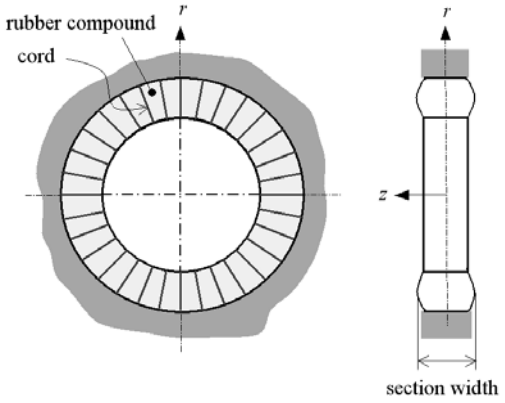

Fig. 2. Sidewall as a composite membrane structure.

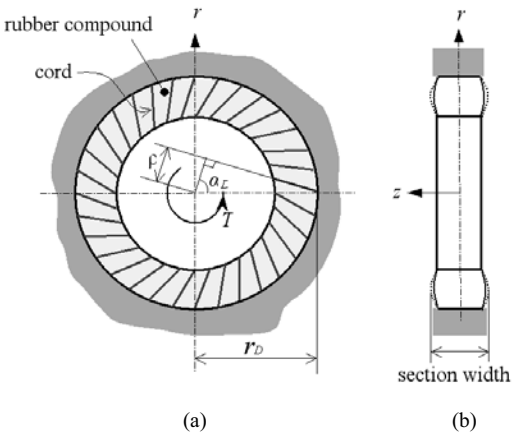

Fig. 3. Deformation of sidewall after torque loading (a) deformation of cord and rubber compound and (b) the contour of sidewall before and after torque loading where the dotted line denotes the contour before deformation and the solid line denotes the contour after deformation.

We will calculate $R(c)$ by using the netting theory and $R(s)$ by employing in-plane shear deformation theory.

3. Formulation of theoretical sidewall contour

The deformation of a tire, which is subjected to an axisymmetric tangential force uniformly distributed along the periphery of the tread, shows shear-dominant axisymmetric deformation in the flexible sidewall. To evaluate the rotational stiffness of the sidewall by using netting theory, it is necessary to describe the cross-section of the sidewall under inflation pressure. Fig. 4 shows a schematic depicting a tire cross-section, where B^*, C, D denote the bead, the turning point and the tread end, respectively, and ϕ_D and α_D signify the meridian angle and cord angle of the tread end, respectively. Akasaka et al. [15] have considered only the cross-section of the flexible sidewall part of a radial tire by introducing a modified bead point of B since the bead center, B^* is located apart from the theoretical curve as shown in Fig. 4. Their netting analysis could be rationalized because the region around the bead center has finite rigidity. They assumed the interval between the two points B^* and B to be rigid while the main part of the sidewall to be a flexible membrane structure. In this paper, we introduce an additional assumption that the modified bead point is somewhere between the outer cord line and inner cord line. This is because the tension due to inflation pressure would be supported by the two cords in the region where two cords are present.

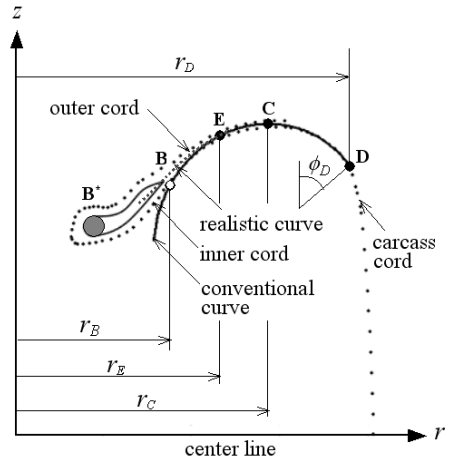

Fig. 4. Comparison between carcass cord (dotted curve), realistic curve and the conventional sidewall contour.

In order to devise a substitute sidewall contour, we divide the interval $r_B \le r \le r_D$ into two domains, that is, the interval $r_B \le r \le r_E$ and the interval $r_E \le r \le r_D$.

We employ the conventional sidewall contour in the interval $r_E \le r \le r_D$ as follows:

$$z(r) = \int_r^{r_D} \frac{A}{\sqrt{B^2 - A^2}} dr + z_D$$
$$= \int_r^{r_D} \frac{r\left(r^2 - r_C^2\right)\sin\phi_D \cdot \sin\alpha_D \left(r^2 - \rho^2\right)^{-1/2}}{\sqrt{\left(r_D^2 - r_C^2\right)^2 - r^2\left(r^2 - r_C^2\right)^2 \sin^2\phi_D \cdot \sin^2\alpha_D \left(r^2 - \rho^2\right)^{-1}}} dr + z_D \tag{6}$$

where

$$A = (r^2 - r_C^{\,2})\sin\phi_D \frac{r\sin\alpha_D}{\sqrt{r^2 - \rho^2}},$$
$$B = r_D^{\,2} - r_C^{\,2},$$
$$\rho = r_D \cos\alpha_D,$$

and z_D is the z-coordinate at $r = r_D$.

Let us introduce the following notations for the sake of convenience.

$$G = B^2 - A^2 \tag{7}$$

and

$$D = (r^2 - \rho^2)G \tag{8}$$

In the interval $r_B \le r \le r_E$, we employ a quadratic curve as a new sidewall contour . The quadratic curve passing through the point E, whose coordinates are (r_E, z_E), is given by

$$\bar{z} = a(r - r_E)^2 + b(r - r_E) + z_E \tag{9}$$

where

$$z_E = z(r_E)$$
$$= \int_{r_E}^{r_D} \frac{A}{\sqrt{B^2 - A^2}} dr + z_D \tag{10}$$

and the coefficients a and b are determined by using the C_1 - and C_2 -continuity conditions at $r = r_E$ as follows:

$$b = -\frac{A_E}{(G_E)^{1/2}} \tag{11}$$

and

$$a = -\frac{1}{2}\frac{B^2}{(G_E)^{3/2}}\left(\frac{\partial A}{\partial r}\right)_E \tag{12}$$

where

$$A_E = A\big|_{r=r_E} = (r_E{}^2 - r_C{}^2)\sin\phi_D \frac{r_E \sin\alpha_D}{\sqrt{r_E{}^2 - \rho^2}} \tag{13}$$

$$\left(\frac{\partial A}{\partial r}\right)_E = \left.\frac{\partial A}{\partial r}\right|_{r=r_E} = \sin\phi_D \bullet \sin\alpha_D \times \frac{2r_E{}^2(r_E{}^2 - r_D{}^2\cos^2\alpha_D) + (r_D)^2\cos^2\alpha_D(r_C{}^2 - r_E{}^2)}{(r_E{}^2 - r_D{}^2\cos^2\alpha_D)^{3/2}} \tag{14}$$

and

$$G_E = G\big|_{r=r_E} = B^2 - (A_E)^2 \tag{15}$$

Additionally, we introduce a parameter ε to make the quadratic curve pass through the point B as follows:

$$\bar{z}(r) = \varepsilon a(r - r_E)^2 + b(r - r_E) + z_E \tag{16}$$

where

$$\varepsilon = \frac{(z_B - z_E) + b(r_E - r_B)}{a(r_B - r_E)^2} \tag{17}$$

which is obtained from the following condition.

$$z_B = \varepsilon a(r_B - r_E)^2 + b(r_B - r_E) + z_E \tag{18}$$

Hence, the new sidewall contour is defined as

$$z(r) = \begin{cases} \int_r^{r_D} \frac{A}{\sqrt{B^2 - A^2}}dr + z_D & for \quad r_E \le r \le r_D \\ \varepsilon a(r - r_E)^2 + b(r - r_E) + z_E & for \quad r_B \le r \le r_E \end{cases} \tag{19}$$

4. Netting theory for rotational stiffness due to cord tension

Consider a differential cord on a deformable composite toroidal membrane structure under inflation pressure p.

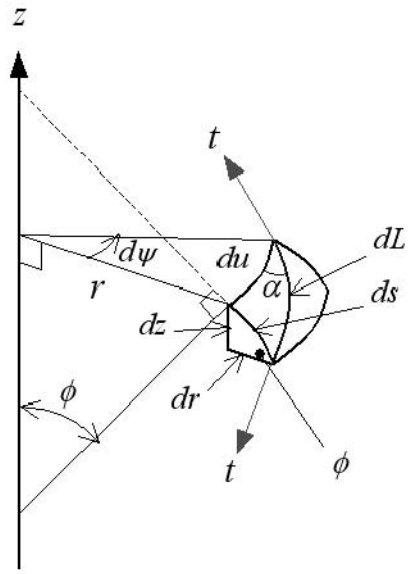

Fig. 5. The cord on a surface, where ds and dL are differential lengths before and after angular deformation $d\psi$, respectively; du is a circumferential displacement; α is a cord angle; and t is the cord tension due to inflation pressure

The differential lengths and angles in Fig. 5 are given by

$$ds = \sqrt{1 + \left(\frac{dz}{dr}\right)^2}\,dr \tag{20}$$

$$= \begin{cases} \frac{B}{\sqrt{B^2 - A^2}}dr & for \quad r_E \le r \le r_D \\ \sqrt{4\varepsilon^2 a^2 (r - r_E)^2 + 4\varepsilon ab(r - r_E) + b^2 + 1}\cdot dr & for \quad r_B \le r \le r_E \end{cases} \tag{21}$$

$$\cos\phi = \frac{dr}{ds} = \left(\frac{ds}{dr}\right)^{-1} = \begin{cases} \frac{\sqrt{B^2 - A^2}}{B} & for \quad r_E \le r \le r_D \\ \frac{1}{\sqrt{4\varepsilon^2 a^2 (r - r_E)^2 + 4\varepsilon ab(r - r_E) + b^2 + 1}} & for \quad r_B \le r \le r_E \end{cases} \tag{22}$$

$$dL = \frac{ds}{\sin\alpha}$$

$$= \begin{cases} \dfrac{B}{\sqrt{B^2 - A^2}} \dfrac{r}{\sqrt{r^2 - \rho^2}} dr, & for \quad r_E \le r \le r_D \\ \sqrt{4\varepsilon^2 a^2 (r - r_E)^2 + 4\varepsilon ab(r - r_E) + b^2 + 1} & \\ \times \dfrac{r}{\sqrt{r^2 - \rho^2}} dr & for \quad r_B \le r \le r_E \end{cases} \tag{23}$$

and

$$d\psi = \frac{du}{r} = \frac{\cot\alpha \cdot ds}{r}$$

$$= \begin{cases} \dfrac{B}{\sqrt{B^2 - A^2}} \dfrac{\rho}{r\sqrt{r^2 - \rho^2}} dr & for \quad r_E \le r \le r_D \\ \sqrt{4\varepsilon^2 a^2 (r - r_E)^2 + 4\varepsilon ab(r - r_E) + b^2 + 1} & \\ \times \dfrac{\rho}{r\sqrt{r^2 - \rho^2}} dr & for \quad r_B \le r \le r_E \end{cases} \tag{24}$$

Then, the cord length is expressed as

$$L = L_1 + L_2 \tag{25}$$

where

$$L_1 = \int_{r_E}^{r_D} \frac{B}{\sqrt{B^2 - A^2}} \frac{r}{\sqrt{r^2 - \rho^2}} dr$$

$$= \int_{r_E}^{r_D} \frac{\left(r_D^{\,2} - r_C^{\,2}\right) r}{\sqrt{D}} dr \tag{26}$$

$$L_2 = \int_{r_B}^{r_E} \sqrt{4\varepsilon^2 a^2 (r - r_E)^2 + 4\varepsilon ab(r - r_E) + b^2 + 1} \times \frac{r}{\sqrt{r^2 - \rho^2}} dr \tag{27}$$

and the rotational angle is expressed as

$$\psi = \psi_1 + \psi_2 \tag{28}$$

where

$$\psi_1 = \int_{r_E}^{r_D} \frac{B}{\sqrt{B^2 - A^2}} \frac{\rho}{r\sqrt{r^2 - \rho^2}} dr$$

$$= \int_{r_E}^{r_D} \frac{\left(r_D^{\,2} - r_C^{\,2}\right) \rho}{r\sqrt{D}} dr \tag{29}$$

$$\psi_2 = \int_{r_B}^{r_E} \sqrt{4\varepsilon^2 a^2 (r - r_E)^2 + 4\varepsilon ab(r - r_E) + b^2 + 1} \times \frac{\rho}{r\sqrt{r^2 - \rho^2}} dr \tag{30}$$

Since the cord tension t is given by [1]

$$t = p\pi \frac{r_D^{\,2} - r_C^{\,2}}{n \cdot \sin\phi_D \cdot \sin\alpha_D} \tag{31}$$

the torque $T(c)$ in Eq. (3) is written as

$$T(c) = \frac{2\pi \cdot p \cdot r_D \left(r_D^{\,2} - r_C^{\,2}\right)}{\sin\phi_D} \cot\alpha_D \tag{32}$$

Since the non-linear relationship between rotational angle ψ and the torque $T(c)$ becomes apparent as ψ increases, the linear rotational stiffness $R(c)$ due to cord tension can be defined by $dT(c)/d\psi$ at $\psi = 0$. Then

$$R(c) = \frac{\dfrac{\partial T(c)}{\partial r_C}\delta r_C + \dfrac{\partial T(c)}{\partial \phi_D}\delta\phi_D + \dfrac{\partial T(c)}{\partial \alpha_D}\delta\alpha_D}{\dfrac{\partial \psi}{\partial r_C}\delta r_C + \dfrac{\partial \psi}{\partial \phi_D}\delta\phi_D + \dfrac{\partial \psi}{\partial \alpha_D}\delta\alpha_D} \tag{33}$$

where

$$\begin{Bmatrix} \delta r_C \\ \delta\phi_D \end{Bmatrix} = \frac{\begin{Bmatrix} \dfrac{\partial z_B}{\partial \phi_D}\dfrac{\partial L}{\partial \alpha_D} - \dfrac{\partial L}{\partial \phi_D}\dfrac{\partial z_B}{\partial \alpha_D} \\ \dfrac{\partial L}{\partial r_C}\dfrac{\partial z_B}{\partial \alpha_D} - \dfrac{\partial z_B}{\partial r_C}\dfrac{\partial L}{\partial \alpha_D} \end{Bmatrix} \delta\alpha_D}{\dfrac{\partial z_B}{\partial r_C}\dfrac{\partial L}{\partial \phi_D} - \dfrac{\partial z_B}{\partial \phi_D}\dfrac{\partial L}{\partial \alpha_D}} \tag{34}$$

The partial derivatives involved in Eqs. (33) and (34) are given in the Appendix.

Eq. (34) is obtained from the fixed condition at B, $\delta z_B = 0$ and the cord inextensibility, $\delta L = 0$, that is,

$$\begin{cases} \delta z_B = \dfrac{\partial z_B}{\partial r_C}\delta r_C + \dfrac{\partial z_B}{\partial \phi_D}\delta\phi_D + \dfrac{\partial z_B}{\partial \alpha_D}\delta\alpha_D = 0 \\ \delta L = \dfrac{\partial L}{\partial r_C}\delta r_C + \dfrac{\partial L}{\partial \phi_D}\delta\phi_D + \dfrac{\partial L}{\partial \alpha_D}\delta\alpha_D = 0 \end{cases} \tag{35}$$

Solving the nonlinear Eq. (35) with the given initial data such as r_C, ϕ_D, and $\alpha_D = \pi/2$, we can determine $R(c) = \left(\dfrac{dT(c)}{d\psi}\right)_{\psi=0}$.

5. Rotational stiffness due to shear deformation of rubber sheets

Applying the in-plane shear deformation theory to the sidewall, which is a composite toroidal membrane structure, Akasaka et al. [15] derived the following rotational stiffness of rubber sheets:

$$R(s) = \frac{T(s)}{\psi} = \frac{1}{\int_{r_B}^{r_D} \frac{1}{4\pi r^3 \cos\phi \cdot G_{eq} \cdot h} dr} \tag{36}$$

where $\cos\phi$ is given by Eq. (22).

Since G_{eq}, $\cos\phi$ and h in Eq. (36) are implicit functions of r, it is impossible to integrate Eq. (36) analytically. To employ numerical integration for Eq. (36), consider a certain cross-section of sidewall shown in Fig. 6. Dividing the cross-section of sidewall, by using lines normal to the carcass cord line, into M parts as shown in Fig. 6, we measured the volume fractions of each rubber compound in the *k*-th part ($V_{[...]}^{(k)}$), the radial coordinates of intersections between carcass cord line and the normal lines to the cord line (r_k and r_{k+1}), and the thickness ($\bar{h}_k$) of the *k*-th part in the normal direction to carcass cord at $r = (r_k + r_{k+1})/2$.

Using the volume fractions of rubber compounds, the equivalent shear modulus of the *k*-th part can be expressed as follows [17]:

$$(G_{eq})_k = \frac{1}{\frac{V_{apex}^{(k)}}{G_{apex}} + \frac{V_{sidewall}^{(k)}}{G_{sidewall}} + \frac{V_{innerliner}^{(k)}}{G_{innerliner}} + \frac{V_{carcass}^{(k)}}{G_{carcass}}} \tag{37}$$

where $G_{[...]}$ denotes shear modulus of the material in brackets.

Assuming the rubber compound is an isotropic material, we have

$$G_{[...]} = \frac{E_{[...]}}{2(1+\nu_m)} \tag{38}$$

where $E_{[...]}$ denotes Young' modulus of the material in the brackets and ν_m denotes Poisson's ratio of rubber compounds, which is assumed as 0.49.

Using the trapezoidal rule, Eq. (36) can be written as

$$R(s) = \frac{1}{\sum_{k=1}^{M} \frac{r_{k+1} - r_k}{4\pi (\bar{r}_k)^3 \cos\bar{\phi}_k \cdot (G_{eq})_k \cdot \bar{h}_k}} \tag{39}$$

where

$$\bar{r}_k = \frac{r_k + r_{k+1}}{2}, \tag{40}$$

$$\cos\bar{\phi}_k = \begin{cases} \dfrac{\sqrt{(r_D^2 - r_C^2)^2 - \dfrac{\bar{r}_k^2 (\bar{r}_k^2 - r_C^2)^2 \sin^2\phi_D \cdot \sin^2\alpha_D}{\bar{r}_k^2 - \rho^2}}}{r_D^2 - r_C^2} & for \quad r_E \le \bar{r}_k \le r_D \\ \dfrac{1}{\sqrt{4\varepsilon^2 a^2 (\bar{r}_k - r_E)^2 + 4\varepsilon ab(\bar{r}_k - r_E) + b^2 + 1}} & for \quad r_B \le \bar{r}_k \le r_E \end{cases} \tag{41}$$

and $\bar{h}_k$ is the thickness of the *k*-th part in the normal direction to carcass cord at $r = \bar{r}_k$. The division of the cross-section of sidewall into parts is shown in Fig. 7.

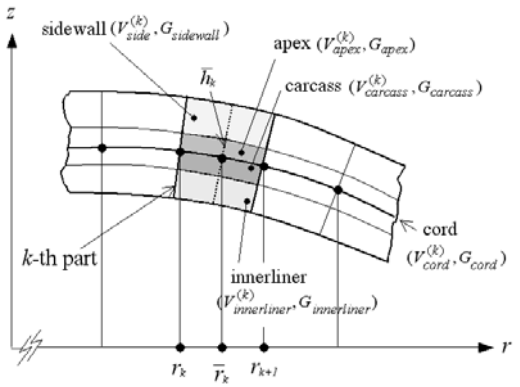

Fig. 6. Rubber compound laminates in the *k*-th part of the sidewall.

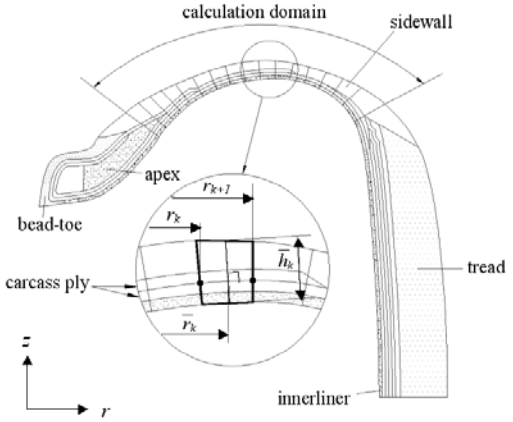

Fig. 7. Structure of sidewall and division of the calculation domain in the sidewall.

6. Results and discussion

A radial tire of P205/60R15 is used to exemplify the present theoretical study. Its dimensions are $r_B = 222mm$, $r_C = 256mm$, $r_D = 283.84mm$ and $\phi_D = 54^o$.

6.1 Sidewall contour fitting

Once the shape of the carcass cord of a tire is given, the first step for the netting analysis is to find the best theoretical fit for the sidewall contour. For example, Fig. 8 shows various conventional fitting curves of the carcass cord, which depend on the value of r_C in Eq. (6), when the values of r_B and ϕ_D are fixed. From Fig. 8, the best fitting is the curve having $r_C = 256mm$ among them but it still deviates from the region between outer and inner carcass cords.

If we use Eq. (19) for curve fitting, we have more parameters such as r_E and z_B to control the theoretical curve or to fit the theoretical curve to the carcass cord than the conventional curve in Eq. (6), which makes it possible to fit the carcass cord more closely. Fig. 9 shows three trial fittings of the carcass cord by Eq. (19). Although Fig. 9 shows improved fittings comparing with the curves in Fig. 8, the fittings in the interval between r_E and r_C are out of the region between the upper and inner cords. This deviation is fixed by using $r_E = 240mm$ and $r_C = 256.5mm$, which is shown in Fig. 10.

The following should be noted: C_1 - and C_2 - continuities of the Eq. (19) at $r = r_E$ are guaranteed when $\varepsilon = 1.0$, while only C_1 -continuity holds unless $\varepsilon = 1.0$. But the present netting theory for rotational stiffness does not require C_2 -continuity of the curve and thus the discontinuity of $\partial^2 z / \partial r^2$ at $r = r_E$ is immaterial especially within the extent of linear theory.

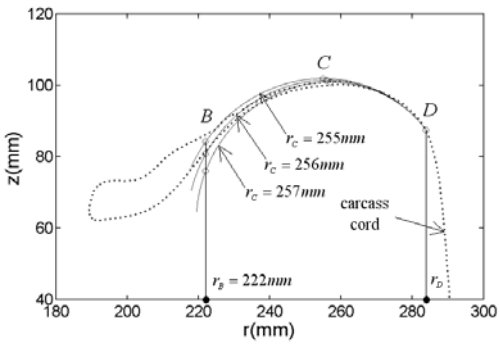

Fig. 8. Conventional curves where $\phi_D = 54^o$ and $r_D = 283.4$ *mm*

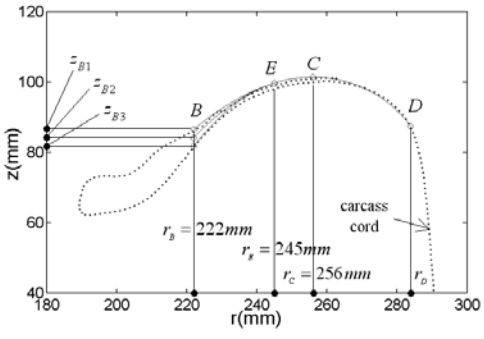

Fig. 9 New trial curves where $\phi_D = 54^o$, $r_D = 283.4mm$, $z_{B1} = 86.52mm$, $z_{B2} = 84.19mm$, and $z_{B3} = 81.85mm$.

6.2 Calculation of rotational stiffness

Young's modulus of each rubber sheet is obtained from the tensile tests of specimens, which are sampled from a real tire [16]. All the necessary geometrical data including volume fractions can be obtained

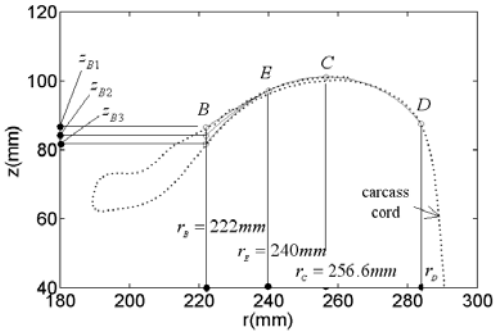

Fig. 10 New optimal curves where $\phi_D = 54^o$, $r_D = 283.4mm$, $z_{B1} = 86.52mm$, $z_{B2} = 84.19mm$, and $z_{B3} = 81.85mm$.

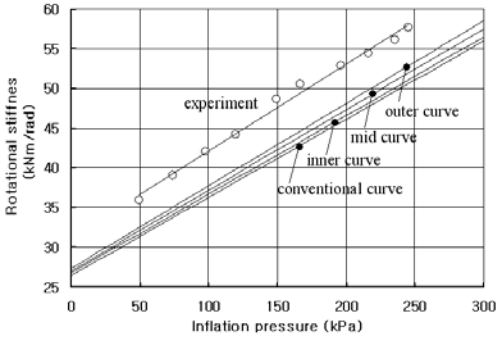

Fig. 11. Rotational stiffness based on the conventional curve with $r_C = 256mm$ shown in Fig. 8 and the three new optimal curves as shown in Fig. 10 (where the outer curve with $z_{B1} = 86.52mm$, the mid curve with $z_{B2} = 84.19mm$, and the inner curve with $z_{B3} = 81.85mm$).

Table 1. The slope of R or $R(c)$ $[kNm/kPa \cdot rad]$.

	Conventional curve	The curves in Fig. 11			Experiment
		Inner curve	Mid curve	Outer curve	
Slope of R or $R(c)$ $[kNm/kPa \cdot rad]$	0.099	0.099	0.102	0.104	0.116

directly from the tire geometry. Then, we can calculate the equivalent shear modulus of the sidewall in each part by using Eq. (37) and the rotational stiffness $R(s)$ by using Eq. (39).

For a sidewall divided into 10 parts, we plot the total rotational stiffness $R = R(c) + R(s)$ versus inflation pressure p in Fig. 11 together with experimental data [17]. Fig. 11 shows that the netting analysis based on new sidewall curves gives closer results to experimental values than the conventional prediction. And the outer fitting curve gives the best result. Especially, we have to pay attention to the fact that the slope of $R(c)$ of the rotational stiffness increases as the theoretical curve is laid more closely to the outer carcass cord as shown in Table 1. The value of the stiffness $R(s)$ due to the rubber sheet also increases as the fitting curve approaches the outer cord. The small variation of $R(s)$ at $p = 0$ comes from the different sidewall contours employed. In the calculation of $R(s)$, each of the three sidewall contours is used as a reference curve for dividing the sidewall into sub-intervals and the sub-intervals are used for calculating the volume fractions of rubber compounds in each sub-interval.

Even though the new sidewall curve improves the result, there is some gap between the theoretical stiffness and the experimental stiffness. This may imply that the value of $R(s)$ is estimated smaller than the real value, that is, the equivalent shear modulus is devaluated because it is difficult to separate the rubber sheet specimens from real tire without any flaws [16].

7. Conclusions

This paper has considered the calculation of the sidewall's rotational stiffness of a radial tire, which is consisted of cord stiffness and rubber compound stiffness. Especially focusing on the calculation of the stiffness due to cord tension, we have introduced a new sidewall contour to represent the real contour more closely and easily than the conventional one. The new sidewall contour is different from the conventional one in that its curve is composite one, i.e., the new sidewall contour is constructed by combining the conventional curve in the interval near to the tread end and the quadratic curve in the interval near to the modified bead point. Since its equation contains more controllable parameters than the conventional one, it is easier to fit the real sidewall contour than the conventional curve. Controlling the parameters contained in the new sidewall contour equation, we can find an adequate curve which is laid between the outer cord and the inner cord easily. The new sidewall contours give improved rotational stiffness of the sidewall compared with the stiffness of the conventional contour, and the value of the stiffness approaches the experimental value as the theoretical curve approaches the outer carcass cord. But there is still some difference between the present prediction and experimental values of rotational stiffness, which may arise from the devaluated shear modulus of each part due to the flaws in the specimens.

References

[1] E. Robecchi and L. Amichi, Mechanics of the inflated tire, *Tire Science and Technology* 1 (3) (1973) 290-345.

[2] R. H. Kennedy, H. P. Patel, and M. S. McMinn, Radial truck tire inflation analysis: theory and experiment, *Rubber Chemistry and Technology* 54 (1982) 751-766.

[3] E. Fiala, Seitenkraft am rollendem Luftreifen, *VDI* 96 (26) (1954) 937-979.

[4] M. Takayama and K. Yamagishi, Simulation model for tire vibration, *Tire Science and Technology* 11 (1) (1984) 38-49.

[5] J. T. Tielking, Plane vibration characteristics of a pneumatic tire model, *SAE* 650492 (1965).

[6] G. R. Potts, C. A. Bell, L. T. Charek, and T. K. Roy, Tire vibrations, *Tire Science and Technology* 5 (4) (1977) 202-225.

[7] T. Kamitamari and H. Sakai, A study on radial tire vibration, *SAE* 852185, (1985) 153-158.

[8] S. C. Huang, and W. Soedel, Effect of Coriolis acceleration on the free and forced in-plane vibrations of rotating rings on elastic foundation, *Journal of Sound and Vibration* 115 (2) (1987) 253-274.

[9] H. Pacejka, Mechanics of Pneumatic Tires, edited by S. K. Clark, U.S. Department of Transportation, Washington D. C., USA, (1981) 726-784.

[10] R. Dohrmann, Dynamics of a tire-wheel-suspen-

sion assembly, *Journal of Sound and Vibration* 205 (5) (1998) 627-642.

[11] R. Dohrmann, Dynamics of a tire-wheel-suspension assembly, *Journal of Sound and Vibration* 205 (5) (1998) 627-642.

[12] J. Padovan, On viscoelasticity and stand waves in tires, *Tire Science and Technology*, 4 (4) (1976) 233.

[13] A. Chatterjee, J. P. Cusumano and J. D. Zolock, On contact-induced standing waves in rotating tires: experiment and theory, *Journal of Sound and Vibration* 227 (5) (1999) 1049-1081.

[14] J. Jenkins, The circumferential contact problem for the belted radial passenger car tire, *Vehicle System Dynamics* 11 (1982) 325-343.

[15] D. S. Stutts and W. Soedel, A simplified dynamic model of the effect of internal damping on the rolling resistance in pneumatic tires, *Journal of Sound and Vibration* 155 (1) (1992) 153-164.

[16] T. Akasaka, S. Yamazaki and K. Asano, An approximate evaluation of rotational stiffness of radial tire, *Transactions of JSCM* 10 (1) (1984) 24-31.

[17] Yong-woo Kim and J. G. Kim, Calculation of sidewall lateral stiffness of a radial tire using material properties of rubber compounds, *Transactions of KSME* 27 (10) (2003) 1667-1675.

[18] Yong-woo Kim and Yongsung Kim, New evaluation and test of sidewall's rotational stiffness of radial tire, *Journal of Mechanical Science and Technology* 20 (6) (2006) 748-758.

Appendix

(1) Partial derivatives of $T(c)$ ***and*** ψ ***:***

$$\frac{\partial T(c)}{\partial r_C} = -\frac{4\pi p r_D r_C}{\sin\phi_D}\cot\alpha_D$$

$$\frac{\partial T(c)}{\partial \phi_D} = -\frac{2\pi p r_D (r_D{}^2 - r_C{}^2)\cot\alpha_D \cos\phi_D}{\sin^2\phi_D}$$

$$\frac{\partial T(c)}{\partial \alpha_D} = -\frac{2\pi p r_D (r_D{}^2 - r_C{}^2)}{\sin\phi_D \cdot \sin^2\alpha_D}$$

$$\frac{\partial \psi}{\partial r_C} = -\int_{r_E}^{r_D} \frac{2\rho r_C}{r D^{1/2}} dr$$

$$+\int_{r_E}^{r_D} \frac{2\rho\left(r_D{}^2 - r_C{}^2\right) r_C \left\{\left(r_D{}^2 - r_C{}^2\right)\left(r^2 - \rho^2\right) - r^2\left(r^2 - r_C{}^2\right)\sin^2\phi_D \cdot \sin^2\alpha_D\right\}}{r D^{3/2}} dr$$

$$+\int_{r_B}^{r_E} \frac{\rho}{r\sqrt{r^2-\rho^2}} \frac{\left\{4\varepsilon^2 a\left(r-r_E\right)^2 + 2\varepsilon b\left(r-r_E\right)\right\}\frac{\partial a}{\partial r_C} + \left\{2\varepsilon a\left(r-r_E\right)+b\right\}\frac{\partial b}{\partial r_C}}{\left\{4\varepsilon^2 a^2\left(r-r_E\right)^2 + 4\varepsilon ab\left(r-r_E\right)+b^2+1\right\}^{1/2}} dr$$

$$\frac{\partial \psi}{\partial \phi_D} = \int_{r_E}^{r_D} \frac{r\left(r_D{}^2 - r_C{}^2\right)\rho\left(r^2 - r_C{}^2\right)^2 \sin\phi_D \cdot \cos\phi_D \cdot \sin^2\alpha_D}{D^{3/2}} dr$$

$$+\int_{r_B}^{r_E} \frac{\rho}{r\sqrt{r^2-\rho^2}} \frac{\left\{4\varepsilon^2 a\left(r-r_E\right)^2 + 2\varepsilon b\left(r-r_E\right)\right\}\frac{\partial a}{\partial \phi_D} + \left\{2\varepsilon a\left(r-r_E\right)+b\right\}\frac{\partial b}{\partial \phi_D}}{\left\{4\varepsilon^2 a^2\left(r-r_E\right)^2 + 4\varepsilon ab\left(r-r_E\right)+b^2+1\right\}^{1/2}} dr$$

$$\frac{\partial \psi}{\partial \alpha_D} = -\int_{r_E}^{r_D} \frac{\left(r_D{}^2 - r_C{}^2\right) r_D \sin\alpha_D}{r D^{1/2}} dr - \int_{r_E}^{r_D} \frac{\left(r_D{}^2 - r_C{}^2\right)^3 r_D{}^3 \cos^2\alpha_D \cdot \sin\alpha_D}{r D^{3/2}} dr$$

$$+\int_{r_E}^{r_D} \frac{\left(r_D{}^2 - r_C{}^2\right) r_D r\left(r^2 - r_C{}^2\right)^2 \sin^2\phi_D \sin\alpha_D \cos^2\alpha_D}{D^{3/2}} dr$$

$$-\int_{r_B}^{r_E} \frac{1}{r}\frac{r_D \sin\alpha_D}{\sqrt{r^2-\rho^2}}\left(1+\frac{\rho^2}{r^2-\rho^2}\right)$$

$$\times\sqrt{4\varepsilon^2 a^2\left(r-r_E\right)^2 + 4\varepsilon ab\left(r-r_E\right)+b^2+1}\, dr$$

$$+\int_{r_B}^{r_E} \frac{\rho}{r\sqrt{r^2-\rho^2}}$$

$$\times \frac{\left\{4\varepsilon^2 a\left(r-r_E\right)^2 + 2\varepsilon b\left(r-r_E\right)\right\}\frac{\partial a}{\partial \alpha_D} + \left\{2\varepsilon a\left(r-r_E\right)+b\right\}\frac{\partial b}{\partial \alpha_D}}{\left\{4\varepsilon^2 a^2\left(r-r_E\right)^2 + 4\varepsilon ab\left(r-r_E\right)+b^2+1\right\}^{1/2}} dr$$

(2) Partial derivatives of

$z_B = \varepsilon a\left(r_B - r_E\right)^2 + b\left(r_B - r_E\right) + z_E$ **:**

$$\frac{\partial z_B}{\partial r_C} = \varepsilon\left(r_B - r_E\right)^2 \frac{\partial a}{\partial r_C} + \left(r_B - r_E\right)\frac{\partial b}{\partial r_C} + \frac{\partial z_E}{\partial r_C}$$

$$\frac{\partial z_B}{\partial \phi_D} = \varepsilon\left(r_B - r_E\right)^2 \frac{\partial a}{\partial \phi_D} + \left(r_B - r_E\right)\frac{\partial b}{\partial \phi_D} + \frac{\partial z_E}{\partial \phi_D}$$

$$\frac{\partial z_B}{\partial \alpha_D} = \varepsilon\left(r_B - r_E\right)^2 \frac{\partial a}{\partial \alpha_D} + \left(r_B - r_E\right)\frac{\partial b}{\partial \alpha_D} + \frac{\partial z_E}{\partial \alpha_D}$$

where

$$z_E = \int_{r_E}^{r_D} \frac{A}{\sqrt{B^2 - A^2}} dr + z_D$$

$$\frac{\partial z_E}{\partial r_C} = -2 r_C \sin\phi_D \sin\alpha_D \int_{r_E}^{r_D}\left[\frac{r}{D^{V2}} - \frac{r(r^2 - r_c^2)}{D^{3/2}}\right.$$

$$\left.\times\{(r_D^2 - r_C^2)(r^2 - r_D^2\cos^2\alpha_D) - r^2(r^2 - r_C^2)\sin^2\phi_D \sin^2\alpha_D\}\right] dr$$

$$\frac{\partial z_E}{\partial \phi_D} = \cos\phi_D \sin\alpha_D \times\left\{\int_{r_E}^{r_D} \frac{r\left(r^2 - r_C^2\right)}{D^{1/2}} dr + \right.$$

$$\left.\sin^2\phi_D \sin^2\alpha_D \int_{r_E}^{r_D} \frac{r^3\left(r^2 - r_C^2\right)^3}{D^{3/2}} dr\right\}$$

$$\frac{\partial z_E}{\partial \alpha_D} = \sin\phi_D \cos\alpha_D \int_{r_E}^{r_D} \frac{r\left(r^2 - r_C^2\right)}{D^{1/2}} dr$$

$$+\sin\phi_D \cdot \cos\alpha_D \cdot \sin^2\alpha_D \times$$

$$\int_{r_E}^{r_D} \frac{r\left(r^2 - r_C^2\right)\left\{r^2\left(r^2 - r_C^2\right)^2 \sin^2\phi_D - r_D{}^2\left(r_D{}^2 - r_C{}^2\right)^2\right\}}{D^{3/2}} dr$$

(3) Partial derivatives of L :

$$\frac{\partial L}{\partial r_C} = -2r_C \int_{r_E}^{r_D} \frac{r}{D^{1/2}} dr$$
$$+2\left(r_D^2 - r_C^2\right) r_C$$
$$\int_{r_E}^{r_D} \frac{r\left\{\left(r_D^2 - r_C^2\right)\left(r^2 - r_D^2\cos^2\alpha_D\right) - r^2\left(r^2 - r_C^2\right)\sin^2\phi_D \cdot \sin^2\alpha_D\right\}}{D^{3/2}} dr$$
$$+\int_{r_B}^{r_E} \frac{\left\{4\varepsilon^2 a\left(r - r_E\right)^2 + 2\varepsilon b\left(r - r_E\right)\right\}\frac{\partial a}{\partial r_C} + \left\{2\varepsilon a\left(r - r_E\right) + b\right\}\frac{\partial b}{\partial r_C}}{\sqrt{4\varepsilon^2 a^2\left(r - r_E\right)^2 + 4\varepsilon ab\left(r - r_E\right) + b^2 + 1}}$$
$$\frac{r}{\sqrt{r^2 - r_D^2\cos^2\alpha_D}} dr$$

$$\frac{\partial L}{\partial \phi_D} = \left(r_D^2 - r_C^2\right)\sin\phi_D \cdot \cos\phi_D \times \sin^2\alpha_D$$
$$\times \int_{r_E}^{r_D} \frac{r^3\left(r^2 - r_C^2\right)^2}{D^{3/2}} dr$$
$$+\int_{r_B}^{r_E} \frac{\left\{4\varepsilon^2 a\left(r - r_E\right)^2 + 2\varepsilon b\left(r - r_E\right)\right\}\frac{\partial a}{\partial \phi_D} + \left\{2\varepsilon a\left(r - r_E\right) + b\right\}\frac{\partial b}{\partial \phi_D}}{\sqrt{4\varepsilon^2 a^2\left(r - r_E\right)^2 + 4\varepsilon ab\left(r - r_E\right) + b^2 + 1}}$$
$$\times \frac{r}{\sqrt{r^2 - r_D^2\cos^2\alpha_D}} dr$$

$$\frac{\partial L}{\partial \alpha_D} = -\left(r_D^2 - r_C^2\right)\sin\alpha_D \cdot \cos\alpha_D$$
$$\times \int_{r_E}^{r_D} \frac{r\left\{\left(r_D^2 - r_C^2\right)^2 r_D^2 - r^2\left(r^2 - r_C^2\right)\sin^2\phi_D\right\}}{D^{3/2}} dr$$
$$+\int_{r_B}^{r_E} \frac{\left\{4\varepsilon^2 a\left(r - r_E\right)^2 + 2\varepsilon b\left(r - r_E\right)\right\}\frac{\partial a}{\partial \alpha_D} + \left\{2\varepsilon a\left(r - r_E\right) + b\right\}\frac{\partial b}{\partial \alpha_D}}{\sqrt{4\varepsilon^2 a^2\left(r - r_E\right)^2 + 4\varepsilon ab\left(r - r_E\right) + b^2 + 1}}$$
$$\times \frac{r}{\sqrt{r^2 - r_D^2\cos^2\alpha_D}} dr$$
$$-r_D^2\cos\alpha_D \cdot \sin\alpha_D$$
$$\times \int_{r_B}^{r_E} \frac{r\sqrt{4\varepsilon^2 a^2\left(r - r_E\right)^2 + 4\varepsilon ab\left(r - r_E\right) + b^2 + 1}}{\left(r^2 - r_D^2\cos^2\alpha_D\right)^{3/2}} dr$$

(4) Partial derivatives of a and b :

$$\frac{\partial a}{\partial r_C} = -\frac{B}{\left(G_E\right)^{3/2}}\frac{\partial B}{\partial r_C}\left(\frac{\partial A}{\partial r}\right)_E$$
$$+\frac{3}{2}\frac{B^2}{\left(G_E\right)^{5/2}}\left(B\frac{\partial B}{\partial r_C} - A_E\frac{\partial A_E}{\partial r_C}\right)\left(\frac{\partial A}{\partial r}\right)_E$$
$$-\frac{1}{2}\frac{B^2}{\left(G_E\right)^{3/2}}\frac{\partial}{\partial r_C}\left\{\left(\frac{\partial A}{\partial r}\right)_E\right\}$$

$$\frac{\partial a}{\partial \phi_D} = \frac{3}{2}\frac{B^2}{\left(G_E\right)^{5/2}}A_E\frac{\partial A_E}{\partial \phi_D}\left(\frac{\partial A}{\partial r}\right)_E - \frac{1}{2}\frac{B^2}{\left(G_E\right)^{3/2}}\frac{\partial}{\partial \phi_D}\left\{\left(\frac{\partial A}{\partial r}\right)_E\right\}$$

$$\frac{\partial a}{\partial \alpha_D} = -\frac{3}{2}\frac{B^2}{\left(G_E\right)^{5/2}}A_E\frac{\partial A_E}{\partial \alpha_D}\left(\frac{\partial A}{\partial r}\right)_E - \frac{1}{2}\frac{B^2}{\left(G_E\right)^{3/2}}\frac{\partial}{\partial \alpha_D}\left\{\left(\frac{\partial A}{\partial r}\right)_E\right\}$$

$$\frac{\partial b}{\partial r_C} = -\frac{\frac{\partial A_E}{\partial r_C}}{\left(G_E\right)^{1/2}} + \frac{A_E\left(B\frac{\partial B}{\partial r_C} - A_E\frac{\partial A_E}{\partial r_C}\right)}{\left(G_E\right)^{3/2}}$$

$$\frac{\partial b}{\partial \phi_D} = -\left(\frac{1}{\left(G_E\right)^{1/2}} + \frac{\left(A_E\right)^2}{\left(G_E\right)^{3/2}}\right)\frac{\partial A_E}{\partial \phi_D}$$

$$\frac{\partial b}{\partial \alpha_D} = -\left(\frac{1}{\left(G_E\right)^{1/2}} + \frac{\left(A_E\right)^2}{\left(G_E\right)^{3/2}}\right)\frac{\partial A_E}{\partial \alpha_D}$$

where

$$\frac{\partial B}{\partial r_C} = -2r_C$$

$$A_E = A\big|_{r=r_E} = \left(r_E^2 - r_C^2\right)\sin\phi_D\frac{r_E\sin\alpha_D}{\sqrt{r_E^2 - r_D^2\cos^2\alpha_D}}$$

$$\frac{\partial A_E}{\partial r_C} = -2r_C\sin\phi_D\frac{r_E\sin\alpha_D}{\sqrt{r_E^2 - r_D^2\cos^2\alpha_D}}$$

$$\frac{\partial A_E}{\partial \phi_D} = \left(r_E^2 - r_C^2\right)\cos\phi_D\frac{r_E\sin\alpha_D}{\sqrt{r_E^2 - r_D^2\cos^2\alpha_D}}$$

$$\frac{\partial A_E}{\partial \alpha_D} = r_E\left(r_E^2 - r_C^2\right)\sin\phi_D$$
$$\times\left\{\frac{\cos\alpha_D}{\sqrt{r_E^2 - r_D^2\cos^2\alpha_D}} - \frac{r_D^2\sin^2\alpha_D\cdot\cos\alpha_D}{\left(r_E^2 - r_D^2\cos^2\alpha_D\right)^{3/2}}\right\}$$

$$\left(\frac{\partial A}{\partial r}\right)_E = \frac{\partial A}{\partial r}\bigg|_{r=r_E}$$
$$= \sin\phi_D\cdot\sin\alpha_D$$
$$\times\frac{2r_E^2\left(r_E^2 - r_D^2\cos^2\alpha_D\right) + r_D^2\cos^2\alpha_D\left(r_C^2 - r_E^2\right)}{\left(r_E^2 - r_D^2\cos^2\alpha_D\right)^{3/2}}$$
$$= \sin\phi_D\cdot\sin\alpha_D\frac{2r_E^4 + \left(r_C^2 - 3r_E^2\right)r_D^2\cos^2\alpha_D}{\left(r_E^2 - r_D^2\cos^2\alpha_D\right)^{3/2}}$$

$$\frac{\partial}{\partial r_C}\left\{\left(\frac{\partial A}{\partial r}\right)_E\right\} = \sin\phi_D\cdot\sin\alpha_D\frac{2r_C r_D^2\cos^2\alpha_D}{\left(r_E^2 - r_D^2\cos^2\alpha_D\right)^{3/2}}$$

$$\frac{\partial}{\partial \phi_D}\left\{\left(\frac{\partial A}{\partial r}\right)_E\right\} = \cos\phi_D\cdot\sin\alpha_D\frac{2r_E^4 + \left(r_C^2 - 3r_E^2\right)r_D^2\cos^2\alpha_D}{\left(r_E^2 - r_D^2\cos^2\alpha_D\right)^{3/2}}$$

$$\frac{\partial}{\partial \alpha_D}\left\{\left(\frac{\partial A}{\partial r}\right)_E\right\} = \sin\phi_D\cdot\cos\alpha_D$$
$$\times\frac{2r_E^4 + \left(r_C^2 - 3r_E^2\right)r_D^2\left(\cos^2\alpha_D - 2\sin^2\alpha_D\right)}{\left(r_E^2 - r_D^2\cos^2\alpha_D\right)^{3/2}}$$
$$-3r_D^2\sin\phi_D\cdot\sin^2\alpha_D\cdot\cos\alpha_D$$
$$\times\frac{2r_E^4 + \left(r_C^2 - 3r_E^2\right)r_D^2\cos^2\alpha_D}{\left(r_E^2 - r_D^2\cos^2\alpha_D\right)^{5/2}}$$